ChemPubSoc Europe

DOI: 10.1002/cctc.201800854

CHEMCATCHEM Full Papers

Insight by In Situ Gas Electron Microscopy on the Thermal Behaviour and Surface Reactivity of Cobalt Nanoparticles

Kassiogé Dembélé,[a, b] Mounib Bahri,[a] Georgian Melinte,[a] Charles Hirlimann,[a] Adrien Berliet,[b] Sylvie Maury,[b] Anne-Sophie Gay,[b] and Ovidiu Ersen*[a, c, d]

Here the thermal behaviour and the surface reactivity of cobalt catalysts supported by alumina-silica and promoted by platinum were investigated by *in situ* transmission electron microscopy (in situ TEM) in a syngas environment. At the standard operating temperature of 220 °C, atomic diffusion and sintering processes onto the support are quite limited on the time scale of the TEM experiment. At temperatures between 350 and 450 °C, particles encapsulation occurred due to a higher CO dissociation and conversion into graphitic layers. Beyond 500 °C, carbon nanotubes (CNTs) growth is activated and the particles undergo (i) morphological changes through continuous elongation and contraction; and (ii) microstructural changes with the appearance of cobalt carbide. By comparing reactions under pure CO and a mixture CO–H_2, it was shown that the addition of dihydrogen to CO increased the rate of CNTs growth and modified the structure of the nanotubes. These results clearly demonstrate the strong ability of the *in situ* TEM to provide the main lines of the reactivity synopsis of nanocatalysts at a nanometric scale under temperature and reactive gas.

Introduction

In the field of heterogonous catalysis, the improvement of the catalysts performances in terms of activity, selectivity and also thermal stability requires a better understanding of their behaviour during their use as actual catalysts. The Fischer-Tropsch synthesis (FTS) reaction is a typical example of a catalytic reaction being presently studied, it allows converting syngas, a mixture of carbon monoxide and dihydrogen into long-chain hydrocarbons.[1,2] The main advantage of this process is to produce high quality hydrocarbon molecules – with no sulphur and nitrogen compounds – from the conversion of natural gas, biomass or coal. In this synthesis, heterogeneous catalysts based on metallic nanoparticles (Fe, Co, Ni, Ru…) dispersed on various supports such as alumina, silica or titania, are generally used. Along with iron, cobalt nanoparticles are the most commonly employed catalysts due to their relatively low price, high stability, and their high selectivity towards linear hydrocarbons. The nominal conditions for their use are high pressures of syngas (up to 4.5 MPa) at a temperature of 220 °C.[1,3] To optimise their thermal stability and to prevent their deactivation, numerous studies using *in situ* and *ex situ* techniques and have been systematically used together with the development of new appropriate characterisation approaches and experimental methodologies.

Among the various methods recently developed or optimised, the transmission electron microscopy (TEM) under controlled atmosphere allows to directly visualise the evolution of nanoparticles during their preparation and subsequent use. In the catalysis field, this is crucial for unfolding the dynamic processes occurring onto the catalysts surface as their modifications during their preparation/operation steps can significantly affect their catalytic performances – i.e. activity, selectivity and stability.

Another key point provided by *in situ* microscopy is the possibility to modify the experimental conditions applied on the specimen (pressure and type of the reactants and/or the temperature used) and to be able to directly depict the consequences. In this manner, one has a nano-laboratory tool for testing the behaviour of catalysts and understanding their interaction with the reactants under specific conditions, which enables one to go one step further than traditional laboratory tools.

Nowadays, two complementary approaches are used to study the catalysts evolution under gas flow: the Environmental TEM[4–6] (ETEM) – also called dedicated ETEM – and windowed gas cell commonly referred to as *in situ* TEM.[7–10] In the ETEM, a modification within the column of the microscope is realised around the specimen area allowing the sample exposure to a maximum pressure of 4 kPa[5]. With the *in situ* TEM, the sample is confined between two electron-transparent windows – usually made out of amorphous silicon nitride membranes –

[a] Dr. K. Dembélé, Dr. M. Bahri, Dr. G. Melinte, C. Hirlimann, Prof. O. Ersen
Institut de Physique et Chimie des Matériaux de Strasbourg (IPCMS)
23 rue du Loess
Strasbourg 67034 (France)
E-mail: Ovidiu.ersen@ipcms.unistra.fr
[b] Dr. K. Dembélé, A. Berliet, Dr. S. Maury, Dr. A.-S. Gay
IFP EnergiesNouvelles
Rond-point de l'8
Changeur de Solaize, 69360 (France)
[c] Prof. O. Ersen
University of Strasbourg, Institute for Advanced Studies (USIAS), 5 allée du Général Rouvillois
Strasbourg 67083 (France)
[d] Prof. O. Ersen
Institut Universitaire de France (IUF)
1 rue Descartes
Paris 75231 (France)

Supporting information for this article is available on the WWW under https://doi.org/10.1002/cctc.201800854

assembled into the tip of a specific holder. Both ETEM and *in situ* TEM can be used not only to directly visualise the catalysts behaviour during their preparation/activation and their evolution under operating conditions but also to provide substantial insight in the deactivation phenomena.[11–13] The *in situ* TEM presents the advantage to directly investigate the catalysts evolution at higher pressure (up to 101.3 – 405.2 kPa),[14] closer to their real-working conditions.

Using the *in situ* TEM in gas environment at atmospheric pressure, we investigated here the thermal behaviour and the surface reactivity of supported cobalt-based nanoparticles. Previous *ex-situ* TEM observation of the supported cobalt catalysts demonstrated their modification during their operation under syngas. For-example Kistamurthy et al.[15] have shown the nanoparticles sintering on Co/SiO_2 catalyst, occurring by Ostwald ripening with the reactor operating at 2.0 MPa of $H_2/CO = 2$ and 230 °C. Other researchers reported, via *ex situ* investigation in similar conditions, the deposition of carbon layers[16,17] over the cobalt particles and the CNTs growth[18] over long-time exposure of the syngas and/or at higher temperature. Both the carbon deposition and CNTs growth are explained by the catalytic conversion of carbon monoxide into carbon layers.[18–20] It has also been shown that the addition of dihydrogen enhances the CNTs growth rate by reducing the rate of deactivation but gives rise to CNTs with a conical structure.[21,22]

Our aim is to directly monitor the processes occurring on the individual nanoparticles morphology and microstructure during the increase of the temperature from 220 °C to 700 °C. The initial catalyst consisting of cobalt oxide particles was first exposed to dihydrogen at atmospheric pressure to obtain the metallic phase. At the particle level, we will track the concomitant morphological and structural changes during the thermal treatment under syngas to draw a reactivity synopsis with the temperature of Co nanograins under syngas.

Results and Discussion

Catalyst in Operation Under Syngas at 220 °C

The cobalt oxide nanoparticles supported by alumina-silica were previously reduced under dihydrogen to allow them to be active for syngas conversion. A representative area of the catalyst is shown in the HAADF-STEM image of Figure 1a. The nanoparticles are observed with a higher HAADF contrast as compared to the one of the support due to the higher atomic number of the cobalt atoms. The subsequent exposure to syngas at a temperature of 220 °C for 1 h is displayed in Figure 1b and showed a slight blurring effect of the image. This is likely due to the presence of hydrocarbon molecules[23] – CO and/or reaction products on the catalyst – which would add diffusion to the electron beam compared to dihydrogen.

During the catalyst operation under syngas, atomic diffusion on the support and a slight particle sintering were detected (see the areas indicated by the arrows). These processes are better emphasised by considering a combined

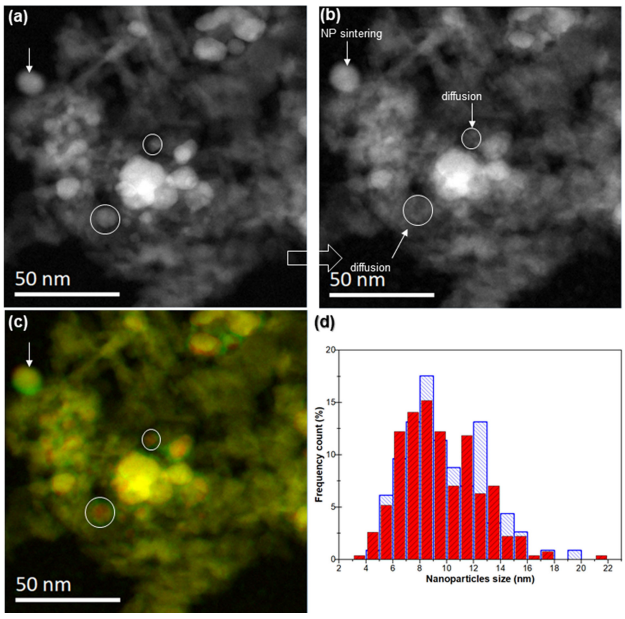

Figure 1. *In situ* HAADF-STEM images of the Co_3O_4-Pt/γ-Al_2O_3-SiO_2 catalyst exposed to H_2 (430 °C, 101.3 kPa) (a) followed by syngas ($H_2/CO = 2$, 220 °C, 101.3 kPa, 1 h) (b). Addition of the coloured images acquired during the exposure to H_2 (coloured in red) and syngas (coloured in green) (c). Nanoparticles size frequency distributions (d) during the exposure to H_2 (red) and syngas at 220 °C (blue). Nanoparticles mean sizes of 9.5 nm were measured under H_2 and 9.8 nm under syngas.

representation of the same area followed under H_2 (coloured in red) and syngas (coloured in green). In this image, shown in Figure 1c, the areas in yellow colour (due to the superposition of red and green) represent the stable areas under both dihydrogen and syngas whereas red and green ones indicate the areas affected by atomic diffusion in the sample.

An overall analysis of the nanoparticles size gives a more global indication about the catalyst stability during the operation under syngas at 220 °C. This was achieved by using a spherical approximation for the morphology of the nanoparticles. The histograms in Figure 1d show the nanoparticles size frequency distribution during the activation under dihydrogen (in red) and their evolution under syngas after 1 h (in blue). The average size of 9.5 nm and 9.8 nm, with a standard deviation of 2.8 nm, were measured on the activated catalyst and after 1 h evolution under syngas, respectively. This indicates a global stability of the catalyst at 220 °C during the first hour. This is not surprising for supported cobalt-based catalysts as the temperature is relatively low[1] to favour nanoparticles migration-coalescence and the expected CO conversion at atmospheric pressure is too low (less than 20%)[24] to allow the particles re-oxidation by the water vapour generated by the reaction.

Nanoparticles Encapsulation by Carbon Graphitic Layers

To study the catalyst deactivation under realistic conditions but under short durations – limited to TEM experiments –, accelerated ageing of the catalysts was attempted by increasing the temperature of the reaction. After 2 h of exposure to syngas at 220 °C, the catalyst behaviour was investigated at higher temperatures of 350 °C-450 °C. Typical bright-field (BF) STEM images of the catalyst at 450 °C are shown in Figure 2. One can

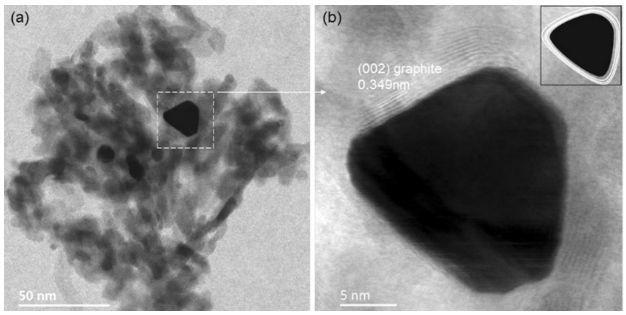

Figure 2. *In situ* BF STEM image of the Co–Pt/γ–Al_2O_3–SiO_2 catalyst exposed to syngas (450 °C, 101.3 kPa) (a). High-resolution BF STEM images of nanoparticles encapsulated by graphitic layers (b). The inset in (b) depicts the observed encapsulation.

observe the presence of faceted nanoparticles on the support. High-resolution BF-STEM images (Figure 3b) of a faceted nanoparticle show its encapsulation by graphitic carbons layers. This is probably related to a higher CO dissociation on the catalyst surface with the increased temperature, facilitating the carbon nucleation and polymerisation. The encapsulation by graphitic layers decreases the number of active sites available on the surface of the particles, leading to their deactivation, in agreement with other previous works.[17,25,26]

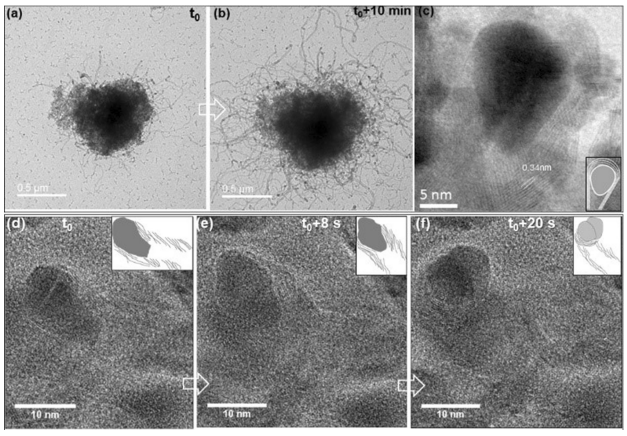

Figure 3. *In situ* TEM image sequence from a recorded movie showing the CNTs formation via tip growth mode on the Co–Pt/γ–Al_2O_3–SiO_2 (a–b). High-resolution BF STEM images showing the particle elongated and encapsulated by graphitic carbon layers (c). The particle deformation during the CNTs growth is depicted in the insets (d–f).

Regarding the nanoparticles encapsulation, two types of scenarios could occur: (i) the carbidic carbon formation[26,27] from the dissociation of carbon monoxide on the nanoparticles surface followed by the carbon nucleation and polymerisation [Eq. (1)]; and/or (ii) the Boudouard reaction [Eq. (2)] in which CO dissociation gives rise to the formation of both carbon dioxide and graphite – this is known as CO disproportionation reaction[27,28].

$$CO \rightarrow C_s + O \quad (1)$$

$$2\ CO \rightarrow CO_2 + C_s \quad (2)$$

At temperature ranging from 350 °C to 450 °C, carbon deposition onto the catalyst surface can simultaneously occur through both processes.[27] Nakamura et al.[29] have evidenced the carbidic carbon formation during the carburization process of a Co/Al_2O_3 catalyst at 230 °C. The authors also reported that a large part of carbidic carbon is decomposed into graphitic carbon when increasing the temperature up to 430 °C. In our case, to identify the products formed on the catalyst, a residual gas analyser equipped with a mass spectrometer was connected to the outlet of the windowed gas-cell holder. The analyser showed an increase in the CO_2 production (see the supplementary information, Figure SI-1) that reaches its maximum at 400 °C. Thus, at this temperature, the Boudouard reaction appears to be the predominant process leading to graphitic layers' formation.

Activation of the Carbon Nanotubes Growth Process

By increasing the temperature up to 500 °C–700 °C, the nanoparticles left the support and CNTs formation proceeded according to the so-called tip growth mode (Figure 3). This is likely favoured by the nanoparticles encapsulation, which can reduce the interaction between the nanoparticles and the support. A similar result for CNTs formation over Co/Al_2O_3 catalysts was reported by Pinheiro et al.[22] during *post-mortem* TEM observation of the CO disproportionation reaction at 600 °C. High temperatures are therefore clearly changing the behaviour of the catalyst. The increase of the temperature can enhance the CO dissociation on the cobalt particle, hence facilitating the carbon dissolution and deviating the reaction selectivity toward the nanotubes formation.

To investigate the CNTs growth mechanism, a real-time monitoring was carried on by recording TEM movies (see the supporting information, SI_video1). As emphasised by the schemes in the insets of Figure 3c–f, graphitic layers are observed in the vicinity of the deformed particle and are inclined with respect to the nanotube axis (herringbone structure), whereas the front of the particles (top surface of the growth direction) remains free of graphitic carbon. While the CNTs growth is going on, new carbon layers are continuously generated on the lateral vicinities of the corresponding particle. This suggests an on-going CO dissociation on the surface of the

particle, thus the availability of the surface to the reactants despite the previous encapsulation at lower temperature. After CO dissociation the carbon atoms may diffuse on the particle surface/subsurface[30–33] or through the bulk[6,34,35] toward the lateral vicinities of the particle constituting the graphitic layers' nucleation and growth sites.

During the CNTs growth process, one can notice that the particle undergoes a morphological change – as depicted by the schemes in the insets of Figure 3d–f – corresponding to a successive elongation and contraction on the rear. This may be related to a structural change, possibly related to a modification in the chemical composition in the vicinity of the particle surface, and/or a metal-liquid like phase transition in the particle. We have therefore followed the nanoparticle reshaping by recording high-resolution TEM (HRTEM) movies. A representative evolution of a nanoparticle microstructure is displayed in Figure 4. Elongated nanoparticles with a potato-like shape are

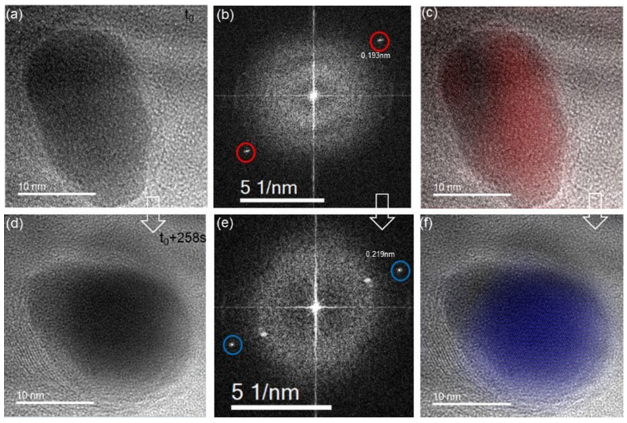

Figure 4. *In situ* BF STEM image of the Co–Pt/γ–Al_2O_3–SiO_2 catalyst exposed to syngas (450 °C, 101.3 kPa) (a). High-resolution BF STEM images of nanoparticles encapsulated by graphitic layers (b). The inset in (b) depicts the observed encapsulation.

observed at the beginning (Figure 4a), followed by a pear-like shape (d). The morphological changes of the particles with elongated and contracted shapes did continue during the CNTs growth. By applying the Fast Fourier Transform (FFT) algorithm on the corresponding images (Figure 4b), a metallic cobalt phase was observed with the presence of {101} hexagonal packing (hcp) plane (see the red circles in b). One minute later, cobalt carbide phases – Co_3C and Co_2C – appeared within the particle. The structural changes were continued with the change in carbidic lattice orientation. For instance, after three minutes, the {002} lattice of Co_2C (see the blue circles in the Figure 4e) was detected when the particle underwent the pear-like shape change. The dynamic process is better emphasised when one adds an inverse FFT image onto the real corresponding image (Figure 4c and f). It is thus clear that the cobalt carbide phases are involved in the CNTs growth and coexist with the metallic phase. The fact that the metallic carbide phase is quite unstable could be at the origin of the morphological fluctuations of the particles during the carbon nanotubes growth process. Similar result on the coexistence of metallic and carbide phases in CNTs growth was reported by Kohigashi et al.[39] during the acetylene decomposition with Co/SiO_2 as a catalyst at low pressure (3 Pa) and 550 °C.

The dynamic structural change of the particle combined to the continuous morphological change could explain the 3D growth of CNTs characterized by several evident modifications in the growth direction, as this would enable a continuous reorientation of rejection plans. In addition, the recurrent deformation of the particles in terms of contraction and elongation of its external shape, very probably leads to a continuous modification of the type and localization of the structural defects on the surface of the particle. This dynamical behaviour was already observed in other previous studies[36], and leads in our case to a variation of the geometrical characteristics of the nanotubes (i.e. diameter and number of graphitic planes) along the tube axis.

From a phenomenological point of view, it has been previously demonstrated that the CNTs can be obtained from various carbon source molecules (C_2H_2, CH_4, CO…).[37,38] All these molecules seem to be more easily decomposed on the defect sites on the surface of the metallic particles than on the atomically flat surfaces.[32,39] However, there is still a strong debate about the possible diffusion processes of the dissociated carbon atoms allowing the subsequent CNTs growth. In this context, from an ETEM study performed on Ni supported MgO catalysts, Helveg et al.[32] deduced that the carbon atoms do principally diffuse on the particle surface toward the graphene-metal interface, without the formation of a carbide phase. Other studies do report the occurrence of sub-surface and bulk diffusion processes of the carbon atoms, even in conditions corresponding to a low activation energy for the surface diffusion, such as for instance the study of Hofmann et al.[33] performed by combining X-ray photoemission spectroscopy and environmental TEM. With respect to these previous studies, in our case which is devoted to the Co catalysts, the presence of both metallic and carbide phases is a good indicator of the subsurface and possible bulk diffusions, without obviously excluding the carbon diffusion on the surface.

Role of the hydrogen in the growth process. The role of the presence of H_2 on the synthesised CNTs morphology, and the rate of their formation were investigated by exposing the catalyst only to pure carbon monoxide at atmospheric pressure. The corresponding results are shown on Figure 5. Once again, the particles encapsulation (Figure 5a) and the CNTs formation (Figure 5b–c) have been confirmed as well as the presence of both metallic cobalt and cobalt carbide. However, the obtained nanotubes were clearly different from the one produced under the CO-H_2 mixture. By measuring the average number of graphene sheets in the CNTs, more graphene sheets were obtained under pure CO compared to the CO-H_2 mixture (11 graphitic planes in average versus 7). This is likely due to the NPs encapsulation which is more important in the absence of H_2. This direct comparison confirms that the dihydrogen molecules do react and assist the carbon layers' decomposition around the particles surface. In addition, we observe that the rate of CNTs growth is three times faster under syngas (~2 μm/

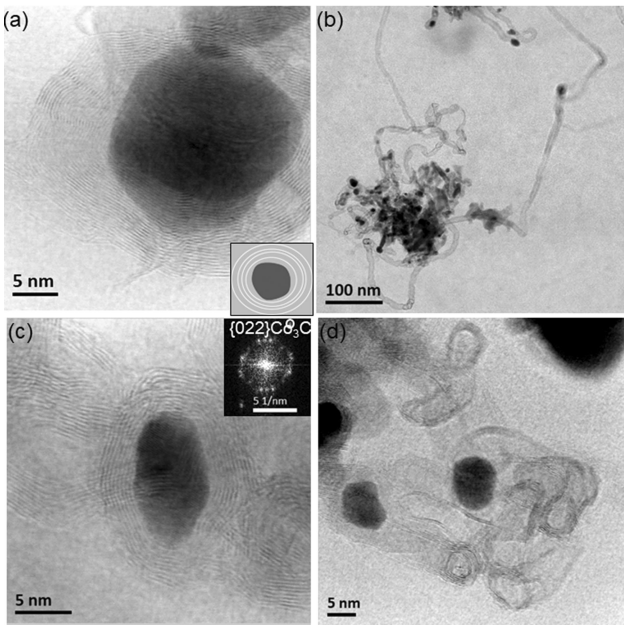

Figure 5. High-resolution BF-STEM image of the particle encapsulation by graphitic layers during the exposure to pure CO (101.3 kPa, 400 °C) of supported cobalt catalyst (a). BF-STEM image showing the CNTs formation at 500 °C (b). The graphitic layers are observed to be parallel to the growth axis as depicted by the scheme in the inset (c). BF-STEM indicating the nanotubes twisted as emphasised by the zoom part (d).

min) compared to the exposure to pure CO (0.7 μm/min). Furthermore, the synthesised carbon nanotubes are more twisted under pure CO (Figure 5d) and a coaxial growth is achieved with the graphene layers which are parallel to the growth axis of the nanotubes (see Figure 5c). This morphological difference in the CNTs with the addition of H_2 to the carbon gas source is in agreement with previous *ex situ* studies.[21,22]

Conclusions

The use of *in-situ* gas TEM provided a direct insight at a nanometric scale on the reactivity behaviour of supported cobalt-based catalysts under syngas at atmospheric pressure. When heating the catalyst up to 220 °C for 2 h, a slight atomic diffusion of the nanoparticles on the support occurred and a global stability of the catalyst was observed on the time-scale of the TEM experiment. At higher temperatures in the range of 400 °C-450 °C, the nanoparticles encapsulation by carbon layers occurred mainly due to the CO disproportionation reaction. On-line mass spectrometry analysis of products of reactions confirmed this reaction by identifying CO_2 formation. By increasing the temperature up to 500–700 °C, the interaction between the particles and the support and the surface reactivity change drastically and the cobalt nanoparticles catalysed the CNTs growth following a tip growth mechanism. During the growth process, continuous morphological and structural changes occurred in the nanoparticles. The cobalt phase was observed to change gradually from metallic to carbide. The formed CNTs structure was found to be different during the exposure to syngas compared to the case of pure CO. In the presence of dihydrogen at high temperature, CNTs with herringbone-structure were grown and a fast CO conversion in the solid graphitic phase was obtained due to a lower particle encapsulation. Whereas under pure CO, the nanotubes grew coaxial and cylindrical and twisted with the graphene layers parallel to the growth axis.

Our results directly show that the temperature play a key role on the interaction between the surface atoms of the cobalt nanoparticles and the reactants. From a general point of view, this study demonstrates that the *in situ* TEM in gas environment at atmospheric pressure is a very appropriate tool for obtaining direct information on the reactivity behaviour of the particles in various gases and along a large temperature domain to be able to study all the possible catalytic reactions.

Experimental Section

The catalyst was prepared via the incipient wetness impregnation of cobalt nitrate in the porosity of silica doped alumina support (Siralox5-type, surface specific area determined by BET about 200 m^2/g, chemical composition 95% Al_2O_3 and 5% SiO_2).[40] First, 8 wt.% of the cobalt salt $\{Co(NH_3)_2, 6H_2O\}$ dispersed in water with 10% ethylene glycol (EG) was deposited in the pores of the support. The EG was used to improve the cobalt dispersion in the support. Then, a second incipient wetness impregnation was realised to obtain a final cobalt content of 14 wt.%. During this second impregnation step, platinum tetraamine hydroxide was added. This is intended to facilitate the cobalt oxide reduction and thereby to enhance the catalyst activity. After each impregnation step, the catalyst was dried at a temperature of 85 °C for a night and calcinated in air at 400 °C for 4 h. The final Co_3O_4-Pt/γ-Al_2O_3-SiO_2 catalyst contained 14 wt.% cobalt and 0.1 wt.% platinum.

For the *in situ* TEM investigation, the catalyst was crushed and the powder was dispersed in ethanol and sonicated for 5 minutes. The experiments were performed with a transmission electron microscope (TEM) JEOL 2100F operating at 200 kV, equipped with a spherical aberration corrector and an UltraScan 1000 CCD array detector. For *in situ* scanning TEM (STEM) studies, a high-angle annular dark-field (HAADF) detector was used, which maximised the collection of incoherent scattered electrons. This enables one to collect images with a high contrast between the nanoparticles and the support since the total detected intensity of the electron beam strongly depends on the atomic number of the specimen ($I \alpha Z^2$), in addition to its thickness.[41] The Protochips Atmosphere windowed gas cell system[7,43] was used, allowing samples exposure at elevated temperatures (up to 1000 °C) and pressures (up to 101.3 kPa).

Before flowing the gas of interest, a cell cleaning was performed by applying several argon flows at 200 °C. Then, the catalyst was exposed to a flow of H_2 gas at atmospheric pressure at 430 °C to reduce the cobalt oxide catalyst. After 2 h of this activation step, the temperature was decreased down to 220 °C, which is the optimum temperature for FTS using cobalt-based catalysts to produce long-chain hydrocarbons.[1] The dihydrogen gas was then substituted with syngas having the gas composition of $H_2/CO = 2$. After 2 h of operations at 220 °C, the temperature was increased by 1 °C/s with a plateau every 50 °C from 350 °C to 700 °C. Dozens of areas of the catalyst have been observed before and during the thermal heating under syngas. To check the effect of the electron beam on the preparation, additional regions – not previously observed – were analysed at the end of the catalyst activation step.

Acknowledgements

K. Dembélé thanks the Region Alsace and IFP Energies Nouvelles for funding his PhD grant. Authors thank the French ANR (National Research Agency) under the 3DClean project 15-CE09-0009-01 for financial support.

Conflict of Interest

The authors declare no conflict of interest.

Keywords: *in situ* TEM · cobalt catalyst · encapsulation · carbon nanotubes

[1] A. Y. Khodakov, W. Chu, P. Fongarland, *Chem Rev* **2007**, *107*, 1692–1744.
[2] A. P. Steynberg, in *Stud. Surf. Sci. Catal.* (Eds.: A. Steynberg, M. Dry), Elsevier, **2004**, pp. 1–63.
[3] M. E. Dry, *Catal. Today* **2002**, *71*, 227–241
[4] J. R. Jinschek, *Chem. Commun.* **2014**, *50*, 2696–2706.
[5] E. D. Boyes, P. L. Gai, *Comptes Rendus Phys.* **2014**, *15*, 200–213.
[6] R. T. K. Baker, *C R C Crit. Rev. Solid State Sci.* **1976**, *6*, 375–399.
[7] L. F. Allard, S. H. Overbury, W. C. Bigelow, M. B. Katz, D. P. Nackashi, J. Damiano, *Microsc. Microanal.* **2012**, *18*, 656–666.
[8] J. F. Creemer, S. Helveg, G. H. Hoveling, S. Ullmann, A. M. Molenbroek, P. M. Sarro, H. W. Zandbergen, *Ultramicroscopy* **2008**, *108*, 993–998.
[9] F. Wu, N. Yao, *Nano Energy* **2015**, *13*, 735–756.
[10] F. (Feng) Tao, P. A. Crozier, *Chem. Rev.* **2016**, *116*, 3487–3539.
[11] K. Dembele, S. Moldovan, C. Hirlimann, J. Harmel, K. Soulantica, P. Serp, B. Chaudret, A.-S. Gay, S. Maury, A. Berliet, O. Ersen, *J. Microsc.* **2018**, *269*, 113–176.
[12] R. T. K. Baker, P. S. Harris, *J. Phys.* **1972**, *5*, 793.
[13] R.-J. Liu, P. A. Crozier, C. M. Smith, D. A. Hucul, J. Blackson, G. Salaita, *Microsc. Microanal.* **2004**, *10*, 77–85.
[14] T. Alan, T. Yokosawa, J. Gaspar, G. Pandraud, O. Paul, F. Creemer, P. M. Sarro, H. W. Zandbergen, *Appl. Phys. Lett.* **2012**, *100*, 081903.
[15] D. Kistamurthy, A. M. Saib, D. J. Moodley, J. W. Niemantsverdriet, C. J. Weststrate, *J. Catal.* **2015**, *328*, 123–129.
[16] K. Fei Tan, J. Xu, J. Chang, A. Borgna, M. Saeys, *J. Catal.* **2010**, *274*, 121–129.
[17] D. J. Moodley, J. van de Loosdrecht, A. M. Saib, M. J. Overett, A. K. Datye, J. W. Niemantsverdriet, *Appl. Catal. Gen.* **2009**, *354*, 102–110.
[18] C.-I. Ahn, H. M. Koo, M. Jin, J. M. Kim, T. Kim, Y.-W. Suh, K. J. Yoon, J. W. Bae, *Microporous Mesoporous Mater.* **2014**, *188*, 196–202.
[19] A. Thaib, G. A. Martin, P. Pinheiro, M. C. Schouler, P. Gadelle, *Catal. Lett.* **1999**, *63*, 135–141.
[20] B. Lee, H. M. Koo, M.-J. Park, B. Lim, D. J. Moon, K. J. Yoon, J. W. Bae, *Catal. Lett.* **2013**, *143*, 18–22.
[21] J. P. Pinheiro, M. C. Schouler, P. Gadelle, *Carbon* **2003**, *41*, 2949–2959.
[22] P. Pinheiro, M. C. Schouler, P. Gadelle, M. Mermoux, E. Dooryhée, *Carbon* **2000**, *38*, 1469–1479.
[23] Y. Li, D. Zakharov, S. Zhao, R. Tappero, U. Jung, A. Elsen, P. Baumann, R. G. Nuzzo, E. A. Stach, A. I. Frenkel, *Nat. Commun.* **2015**, *6*, 7583.
[24] W. Chu, P. A. Chernavskii, L. Gengembre, G. A. Pankina, P. Fongarland, A. Y. Khodakov, *J. Catal.* **2007**, *252*, 215–230.
[25] A. M. Saib, D. J. Moodley, I. M. Ciobîcă, M. M. Hauman, B. H. Sigwebela, C. J. Weststrate, J. W. Niemantsverdriet, J. van de Loosdrecht, *Catal. Today* **2010**, *154*, 271–282.
[26] C. H. Bartholomew, *Appl. Catal. Gen.* **2001**, *212*, 17–60.
[27] J. Nakamura, I. Toyoshima, K. Tanaka, *Surf. Sci.* **1988**, *201*, 185–194.
[28] G. M. Bremmer, E. Zacharaki, A. O. Sjåstad, V. Navarro, J. W. M. Frenken, P. J. Kooyman, *Faraday Discuss.* **2017**, *197*, 337–351.
[29] J. Nakamura, K. Tanaka, I. Toyoshima, *J. Catal.* **1987**, *108*, 55–62.
[30] C. T. Wirth, S. Hofmann, J. Robertson, *Diam. Relat. Mater.* **2009**, *18*, 940–945.
[31] F. Abild-Pedersen, J. K. Nørskov, J. Rostrup-Nielsen, J. Sehested, S. Helveg, *Phys. Rev. B Condens. Matter.* **2006**, *73*, 115419.
[32] S. Helveg, C. López-Cartes, J. Sehested, P. L. Hansen, B. S. Clausen, J. R. Rostrup-Nielsen, F. Abild-Pedersen, J. K. Nørskov, *Nature* **2004**, *427*, 426–429.
[33] S. Hofmann, G. Csányi, A. C. Ferrari, M. C. Payne, J. Robertson, *Phys. Rev. Lett.* **2005**, *95*, 036101.
[34] J. Rostrup-Nielsen, D. L. Trimm, *J. Catal.* **1977**, *48*, 155–165.
[35] N. M. Rodriguez, *J. Mater. Res.* **1993**, *8*, 3233–3250.
[36] H. Yoshida, S. Takeda, *Carbon* **2014**, *70*, 266–272.
[37] R. T. K. Baker, M. A. Barber, P. S. Harris, F. S. Feates, R. J. Waite, *J. Catal.* **1972**, *26*, 51–62.
[38] M. Kumar, Y. Ando, *Carbon Nanotube Synthesis and Growth Mechanism*, INTECH Open Access Publisher, **2011**.
[39] S. Esconjauregui, C. M. Whelan, K. Maex, *Carbon* **2009**, *47*, 659–669.
[40] L. Braconnier, E. Landrivon, I. Clémençon, C. Legens, F. Diehl, Y. Schuurman, *Catal. Today* **2013**, *215*, 18–23.
[41] K. Sohlberg, T. J. Pennycook, W. Zhou, S. J. Pennycook, *Phys Chem Phys* **2015**, *17*, 3982–4006.
[42] "Protochips | In Situ TEM Holders and SEM Stages," can be found under http://www.protochips.com/products/atmosphere/, **2017**.
[43] B. Jager, R. Espinoza, *Catal. Today* **1995**, *23*, 17–28.

Manuscript received: May 25, 2018
Accepted Article published: July 6, 2018
Version of record online: July 24, 2018